# Source localization using rational approximation on plane sections



2012 Inverse Problems 28 055018

(http://iopscience.iop.org/0266-5611/28/5/055018)

Inverse Problems 28 (2012) 055018 (24pp) doi:10.1088/0266-5611/28/5/055018

# Source localization using rational approximation on plane sections

**M Clerc**[1], **J Leblond**[2], **J-P Marmorat**[3] **and T Papadopoulo**[1]

[1] Athena project-team, INRIA Sophia Antipolis Méditerranée, France
[2] Apics project-team, INRIA Sophia Antipolis Méditerranée, France
[3] CMA, École des Mines de Paris, Sophia Antipolis, France

E-mail: Maureen.Clerc@inria.fr, Juliette.Leblond@inria.fr, Jean-Paul.Marmorat@ensmp.fr and Theodore.Papadopoulo@inria.fr

Received 29 August 2011, in final form 1 September 2011
Published 23 April 2012
Online at stacks.iop.org/IP/28/055018

**Abstract**
In functional neuroimaging, a crucial problem is to localize active sources within the brain non-invasively, from knowledge of electromagnetic measurements outside the head. Identification of point sources from boundary measurements is an ill-posed inverse problem. In the case of electroencephalography (EEG), measurements are only available at electrode positions, the number of sources is not known in advance and the medium within the head is inhomogeneous. This paper presents a new method for EEG source localization, based on rational approximation techniques in the complex plane. The method is used in the context of a nested sphere head model, in combination with a cortical mapping procedure. Results on simulated data prove the applicability of the method in the context of realistic measurement configurations.

*In memory of Line Garnero, and of her communicative dedication to unveiling the mysteries of the brain.*

(Some figures may appear in colour only in the online journal)

## 1. Introduction

Electromagnetic source mapping aims at localizing active sources within the brain from measurements of the electromagnetic field they produce, which can be measured passively outside the head. This paper deals more specifically with the electric potential which is measured using electroencephalography (EEG).

Estimating neural current sources located within the brain from outside measurements falls into a category of inverse source problems, that are severely ill-posed in general, mainly due to the lack of continuity and stability, but also to non-uniqueness (Isakov 1998, Vessella 1992).

When a limited number of sources are modeled as pointwise and dipolar, there are in general more measurements than unknowns, and it has been proved that the inverse problem of source estimation has a unique solution (El Badia and Ha-Duong 2000). However, even in this pointwise and dipolar case, solutions to the inverse source problem are often unstable, in particular with respect to the number of sources.

Several families of methods exist to solve the inverse source localization problem, when sources can be modeled as the superposition of a small number of dipoles (Scherg *et al* 1999). *Dipole fitting* methods must minimize a non-convex goal function, yielding an outcome that is unstable with respect to the number of dipoles in the model (Cuffin 1995). Whenever this number is assumed to be known *a priori*, an algebraic (scanning) method has been proposed in El Badia and Ha-Duong (2000), which requires rank computation of related matrices. In practice, one does not know this number in advance, and learning this model order is far from trivial (Bénar *et al* 2005). If the sources are decorrelated in time, analyzing the covariance matrix of the measured data provides an estimate of the number of active dipoles. The number of sources is indeed equal to the number of singular values that are significantly different from zero. The *MUSIC method* first applies a principal component analysis (PCA) to the measurements, and then identifies a 'signal subspace' the analysis of which subsequently determines the dipole positions (Mosher *et al* 1992). In practice, the dimensionality of the signal subspace is difficult to determine, and the dipoles are extracted one at a time by seeking the global maximum of a contrast function among all possible source positions. *MUSIC* can thus only be applied if the sources are well modeled by a small number of asynchronous dipoles. With the stronger assumption of decorrelated sources, another method, *beamforming*, can also estimate active sources, by scanning a region of interest, and by comparing the covariance of the measurement to that of the baseline, measured in time windows that do not contain the activity of interest (Van Veen and Buckley 1988).

This paper proposes a new approach, which, like *MUSIC* and *beamforming*, requires no prior information on the number of sources. However, unlike *MUSIC* or *beamforming*, which require as input consecutive measurements within a time window, the proposed method works instant by instant, and *a fortiori* does not require sources to be decorrelated across time.

Our method belongs to a new category of source estimation algorithms that are grounded in harmonic analysis and best approximation theory, and offer stability (Baratchart *et al* 2006, Kandaswamy *et al* 2009). These analytical methods directly localize the sources as the singularities of the potential from boundary measurements.

The types of geometry and boundary data that they require do not necessarily coincide with actual measurements. Indeed, these methods usually work in a homogeneous domain, and an explicit parametrization may be needed for its boundary.

We present our constructive approach to this inverse problem, in the framework of a (classical) spherical geometry. Under quasi-static assumptions, Maxwell's equations lead to a formulation of the electric potential $u$ as a solution to Laplace's equation. In the innermost layer (the brain), there may be singularities due to the presence of current sources. These singularities are to be localized from available data on the outer boundary (the scalp). The core of our inverse solution relies on approximation schemes that are meant to operate inside homogeneous domains, and not in such a nested geometry. Hence, a preliminary stage consists of mapping to the cortex the data initially measured on the surface of the scalp. This *cortical mapping* problem is a Cauchy (transmission) problem for the Laplace operator (Clerc and Kybic 2007).

Source detection from cortical data is another classical inverse problem for the Laplace operator, which consists of recovering an unknown number of pointwise sources within a homogeneous domain from measurements of the potential and its normal derivative on the boundary.

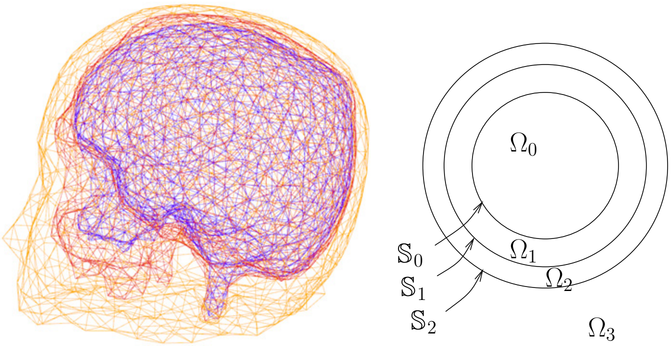


**Figure 1.** A nested conductor model for the head (left), in which brain, skull and scalp have a homogeneous conductivity. Our 3D spherical nested model (right, 2D view), where the brain and scalp ($\Omega_0$, $\Omega_2$) conductivity is 0.33, the skull conductivity is 0.0042 and the air $\Omega_3$ is non-conductive.

When the domain is a spherical ball, then the above issue is equivalent to a sequence of 2D inverse problems, each of which consists of recovering the singularities of some function $f$ in a disk from the knowledge of $f$ on the boundary circle (Baratchart *et al* 2006). Consequently, we apply to these 2D problems a technique inspired by that described in Baratchart *et al* (2005) that relies on approximating $f$ on the boundary circle by a rational function with poles in the disk.

Finally, we locate the singularities by analyzing the cluster of these poles. Geometrical restriction to spherical domains allows one to make explicit (and not too complex, in a preliminary feasibility study) the behavior of the 2D singularities with respect to the 3D sources, which is granted by our recovery scheme.

The outline is as follows: section 2 introduces the inverse problem and section 3 presents the solution proposed in this paper. Section 4 demonstrates the method on numerical examples. The paper also includes a conclusion in section 5 and technical appendices that detail some mathematical aspects of the method.

## 2. The inverse problem

### 2.1. Model setting

In a simplified spherical model, the head is assumed to be the union of three disjoint homogeneous spherical layers[4] $\Omega_0$, $\Omega_1$, $\Omega_2$, namely the brain, the skull and the scalp, within a non-conductive medium $\Omega_3$ representing the air. Up to a rescaling, one may assume the ball $\Omega_0$ representing the brain to have radius 1 and to be centered at the origin. The spheres separating the volumes $\Omega_i$ are denoted as $\mathbb{S}_0$, $\mathbb{S}_1$ and $\mathbb{S}_2$ (see figure 1). The conductivity in each $\Omega_i$ is denoted by $\sigma_i$. For simplicity and without loss of generality, we assume that $\sigma_0 = 1$. Then, we define a piecewise constant function $\sigma$ in $\mathbb{R}^3$ by $\sigma_{|\Omega_i} = \sigma_i$. The current sources are modeled as dipoles situated strictly inside the inner layer $\Omega_0$ and are characterized by their number $n$, their positions $C_k \in \Omega_0$ and their moments $p_k \in \mathbb{R}^3$, $k = 1, \ldots, n$.

[4] In the remainder of this paper, all domains are supposed to be open.

### 2.2. The inverse problem

The potential created by the dipolar sources $(C_k, p_k)$ located inside $\Omega_0$ is a solution to the forward problem

$$\text{(FP)} \qquad \begin{cases} \nabla \cdot (\sigma \nabla u) = \mathcal{S} = \displaystyle\sum_{k=1}^{n} p_k \,.\, \nabla \delta_{C_k} \text{ in } \mathbb{R}^3 \\ \sigma \partial_\nu u_{|\mathbb{S}_2} = 0 \text{ (current flux),} \end{cases} \tag{1}$$

where $\nu$ denotes the outward unit normal vector to the surfaces. The homogeneous Neumann boundary condition is due to the fact that the outer medium (air) is non-conductive. The current flowing through the neck is neglected.

Let $K$ denote a set of points on $\mathbb{S}_2$, representing electrode positions. The inverse source localization problem (IP) associated with the forward problem (FP) is then as follows.

(IP) *Given measurements of $u$ on $K$, find the number of unknown pointwise dipolar sources, their positions $C_k \in \Omega_0$ and their moments $p_k \in \mathbb{R}^3$, such that $u$ satisfies (FP).*

### 2.3. Properties of solutions to (IP)

Mathematical properties of (IP) have been established when the data are known in an open subset $K$ of the boundary. In our case, the data are only known on a discrete set, but it is assumed that the underlying potential is smooth enough so that it is well approximated on an open set $K$ from the data. Uniqueness of solutions to (IP) (identifiability from boundary measurements) has been established in El Badia and Ha-Duong (2000). If two finite distributions of pointwise dipolar sources generate the same potential on some open subset $K$ of $\mathbb{S}_2$, then they are identical.

Stability properties for (IP) may only hold for smooth enough boundary data on $K$ (in Sobolev spaces). This is due to the classical ill-posedness of Cauchy-type issues (section 3.1.1) (Alessandrini *et al* 2009, Isakov 1998, Phung 2003, Zghal 2010). Concerning the source problem in the homogeneous domain (sections 3.3 and 3.4), stability results are established in El Badia (2005) and Vessella (1992).

## 3. Solution to the inverse problem (IP)

The resolution of the above inverse problem (IP) consists of two main steps as represented in the flowchart in figure 2.

*Data transmission* from $\mathbb{S}_2$ to $\mathbb{S}_0$, which involves the following.

- *Cortical mapping* (section 3.1.1). The data are transmitted from the surface of the scalp $\mathbb{S}_2$ where it is measured (on electrodes) onto the surface $\mathbb{S}_0$ of the brain.
- *Harmonic projection* (section 3.1.2). Filtering out possible outer sources by keeping only the information related to the effective inner sources in $\Omega_0$.

*Source recovery* in $\Omega_0$ from data on $\mathbb{S}_0$, which involves the following.

- *Plane sections* (section 3.2). The sphere $\mathbb{S}_0$ is sliced along families of parallel planes, perpendicular to a chosen axis, yielding disks inside which the singularities will be sought.
- *Planar singularity detection* (section 3.3). 2D approximation techniques are used to find the planar singularities on the plane sections of $\Omega_0$ (disks).
- *3D source localization* (section 3.4). For a putative number of sources, the sources are localized in 3D by analyzing the sets of planar singularities.

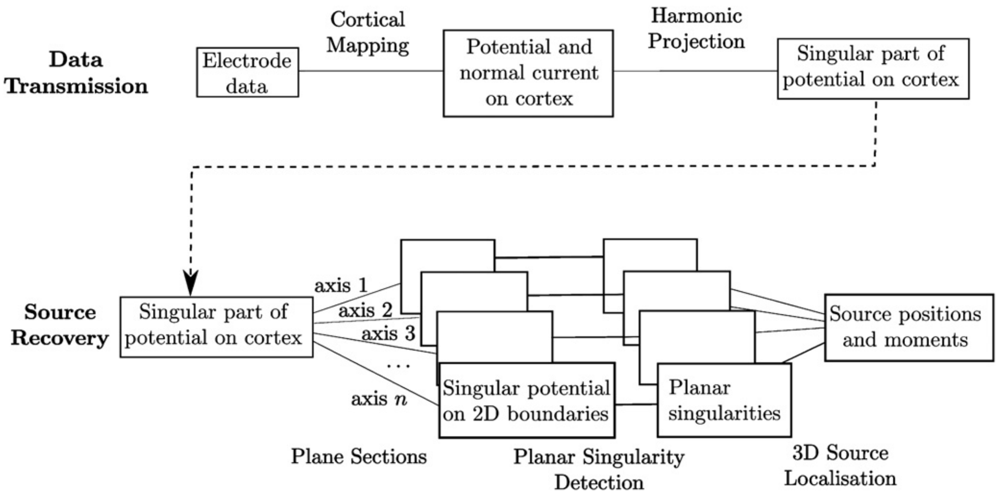


**Figure 2.** Flowchart of the source localization method, consisting of two main steps: data transmission and source recovery. Source recovery makes use of a 2D rational approximation technique, which is run independently on slices of the domain. The planar singularities are then analyzed jointly to yield the positions and moments of the sources.

The data transmission step uses the approach proposed in Clerc and Kybic (2007), while the source recovery step uses the one described in Baratchart *et al* (2006) (see also Ben Abda *et al* (2009), in two dimensions).

### *3.1. Data transmission*

*3.1.1. Cortical mapping.* The goal, as recalled in figure 2, is to estimate the values of the potential and the normal current on the cortex, from the values on electrodes of a potential that satisfies the forward problem (1). This forward problem can be decomposed in each of the three layers $\Omega_i$, $i = 0, 1, 2$. By assumption, there are no sources outside the inner volume $\Omega_0$; hence, the potential $u$ satisfies a homogeneous Laplace equation in the layers $\Omega_1$ and $\Omega_2$:

$$\Delta u = 0 \text{ in } \Omega_i, \qquad i = 1, 2.$$

The continuity of the potential and of the normal current across the interfaces are expressed through the following transmission conditions:

$$u^+ = u^- \text{ on } \mathbb{S}_i, \qquad i = 0, 1, \tag{2}$$

$$\text{and } \sigma_{i+1}\partial_\nu u^+ = \sigma_i \partial_\nu u^- \text{ on } \mathbb{S}_i, \qquad i = 0, 1, \tag{3}$$

where the superscripts + and − indicate the limiting values when approaching $\mathbb{S}_i$ from $\Omega_{i+1}$ (outside) and $\Omega_i$ (inside), respectively.

The data transmission problem which we aim to solve is a Cauchy problem (CP), for $u$ harmonic within $\Omega_1$ and $\Omega_2$, satisfying the transmission conditions (2) and (3).

(CP) *Given measurements* $u_K$ *of* $u$ *on* $K \subset \mathbb{S}_2$ *and given that* $\partial_\nu u = 0$ *on* $\mathbb{S}_2$*, find the values* $g = u_{|\mathbb{S}_0}$ *and* $\phi = \partial_\nu u^-_{|\mathbb{S}_0}$ *on* $\mathbb{S}_0$.

Solving (CP) is non-trivial, because the Cauchy problem for the Laplace equation is the prototype of an ill-posed problem. Indeed, (CP) has similar stability properties to those described in section 2.3 for $K \subset \mathbb{S}_0$. Regularization schemes have been proposed in Atfeh *et al* (2010) and Kozlov *et al* (1992). We solve the cortical mapping with a regularized Tikhonov method deriving from a 'boundary elements' formulation of the problem (this step is thus not limited to spherical interfaces): from its values $u_K$ on the measurement set $K$, $u$ is estimated, along with $\sigma \partial_\nu u$, on the three surfaces $\mathbb{S}_2$, $\mathbb{S}_1$ and $\mathbb{S}_0$. This method, originally presented in Clerc and Kybic (2007), is detailed in appendix A.

*3.1.2. Harmonic projection (in $\mathbb{R}^3$).* After the cortical mapping step has provided the potential $g = u$ and its normal derivative $\phi = \partial_\nu u$ on the surface of the cortex $\mathbb{S}_0$, the potential $u$ satisfies in $\Omega_0$ an equation of the form

$$\begin{cases} \Delta u = \mathcal{S} = \displaystyle\sum_{k=1}^{n} p_k \,.\, \nabla \delta_{C_k} \text{ in } \Omega_0, \\ \partial_\nu u = \phi, \quad u = g \text{ on } \mathbb{S}_0. \end{cases} \tag{4}$$

From $g$ and $\phi$ on $\mathbb{S}_0$, we first look for the part $u_a$ of the potential $u$ which is harmonic outside the ball $\Omega_0$, vanishes at $\infty$ and still contains on $\mathbb{S}_0$ all the information on the distribution of sources.

Knowing that the potential $u$ in $\Omega_0$ is a solution of (4), let $u_a$ be the convolution of $\mathcal{S}$ with the Green function for the Laplacian in $\mathbb{R}^3$:

$$u_a(x) = \sum_{k=1}^{n} \frac{\langle p_k,\ x - C_k \rangle}{4\pi |x - C_k|^3}, \qquad x \neq C_k, \tag{5}$$

where the brackets $\langle , \rangle$ denote the scalar product in $\mathbb{R}^3 \times \mathbb{R}^3$. Note that

$$\Delta u_a = \Delta u = \mathcal{S} \text{ in } \Omega_0,$$

$$\text{while } \Delta u_a = 0 \text{ in } \mathbb{R}^3 \setminus \Omega_0, \text{ and } \lim_{|x| \to \infty} |u_a(x)| = 0.$$

Consequently, for $x \in \Omega_0 \setminus \{C_k\}$, we have

$$u(x) = h(x) + u_a(x) = h(x) + \sum_{k=1}^{n} \frac{\langle p_k,\ x - C_k \rangle}{4\pi |x - C_k|^3},$$

for a harmonic function $h$ in $\Omega_0$.

In practice, $u_a$ is computed from the available boundary data $g$ and $\phi$ on $\mathbb{S}_0$ by expanding $u$ there on the basis of spherical harmonics (Baratchart *et al* 2006, Dautray and Lions 2000). Indeed, $u$ being a harmonic function in a neighborhood of $\mathbb{S}_0$, the coefficients of its expansion on $\mathbb{S}_0$ of negative indices coincide with those of $u_a$. They are given through a linear system, by identification with the coefficients of the spherical harmonics expansions of the discretized $g$ and $\phi$ on $\mathbb{S}_0$.

Figure 3 shows the singular part $u_a$ of the potential, computed from its expression (5) on $\mathbb{S}_0$, from $n = 2$ sources $C_1 = (0.5, 0.5, 0.5), C_2 = (0.5, -0.5, -0.4)$ with moments $p_1 = (1, 1, 1), p_2 = (-1, 1, 1)$.

### 3.2. From 3D to 2D

Given $u_a$, we can now formulate an *inverse source recovery problem* in $\Omega_0$.

(SP) *Given $u_a$ on $\mathbb{S}_0$, find the number of unknown pointwise dipolar sources, their locations $C_k \in \Omega_0$ and their moments $p_k \in \mathbb{R}^3$, such that $u_a$ satisfies (5).*

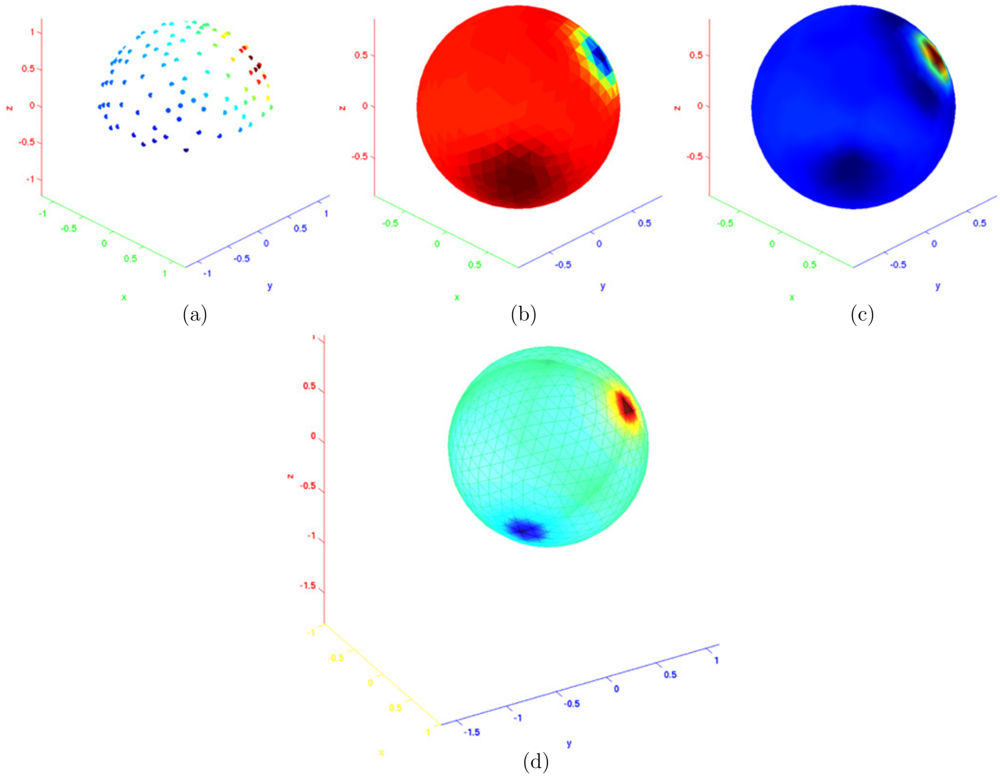


**Figure 3.** Data transmission. Cortical mapping: from electrode data (a), yielding the normal current (b) and the potential (c) on the cortical surface. Harmonic projection: (d) representation on the cortex $\mathbb{S}_0$ of the singular part $u_a$ of the potential, whose singularities are restricted to $\Omega_0$.

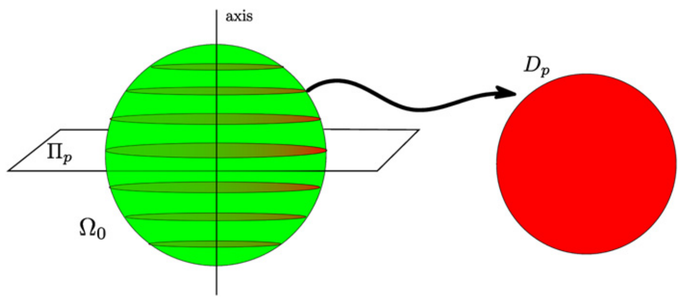


**Figure 4.** Plane sections. $\Omega_0$ is sliced into disks $D_p$ by a series of parallel planes $\Pi_p$.

Following Baratchart *et al* (2006), we first study the singularities of $u_a^2$ on plane sections of $\Omega_0$, where the function can be analytically extended to the complex plane.

The ball $\Omega_0$ is sliced along a family of $P$ planes, $\Pi_p$, $p = 1, \ldots, P$, parallel to some plane $\Pi \subset \mathbb{R}^3$ (see figure 4). The intersections of the planes $\Pi_p$ with $\Omega_0$ are disks $D_p$, whose boundaries are circles $T_p$ (intersections $\Pi_p \cap \mathbb{S}_0$). The data transmission step (section 3.1) has provided the singular part $u_a$ of the potential on $\mathbb{S}_0$, and we now consider its restriction to each circle $T_p$.

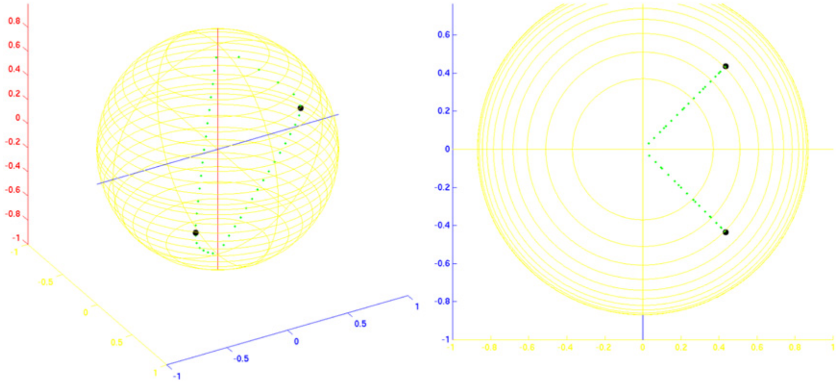

**Figure 5.** True sources $C_1, C_2$ (large black dots) and theoretical singularities $s_{1,p}, s_{2,p}$, $p = 1, \ldots, P$, which when joining the small light grey (green) dots form singular lines $l_k$ (see section 3.4): 3D view (left), top view (right).

The computations that follow are detailed in appendix B. Denote by $(x_1, x_2, x_3)$ the Cartesian coordinates in $\mathbb{R}^3$. Choose for simplicity $\Pi = \{x_3 = 0\}$ (this is always possible by composition with a rotation) whence $\Pi_p = \{x_3 = x_{3,p}\}$. For some fixed $x_{3,p} \in (-1, 1)$, let

$$x \in T_p : \quad x = (x_1, x_2, x_{3,p}), \qquad r_p = \sqrt{1 - x_{3,p}^2}, \qquad z = (x_1 + \mathrm{i}x_2)/r_p, \tag{6}$$

where $r_p$ is the radius of the circle $T_p$, and $z \in T$ is the normalized complex affix associated with $x \in T_p$.

From $u_a$ on $T_p$, we build the *complex variable* function $f_p$ on the unit circle $T \subset \mathbb{C}$ (the complex plane) as follows:

$$f_p(z) = u_a^2(x_1, x_2, x_{3,p}). \tag{7}$$

For fixed $p$, the function $f_p$ coincides with the trace on $T$ of a function defined on $\mathbb{C}$ except at singularities: due to the $n$ sources $C_k$, this extended function (that we still call $f_p$) has $n$ singularities inside the unit disk $D$ (as well as $n$ related singularities outside the closed disk $\overline{D}$).

Indeed, let us denote the source coordinates by $C_k = (x_{1,k}, x_{2,k}, x_{3,k})$, and their corresponding complex affix by $z_k = x_{1,k} + \mathrm{i}x_{2,k}$, for $k = 1, \ldots, n$. Assuming $z_k \neq 0$[5], we have from (5), (7), at $x \in T_p$ and corresponding complex affix $z \in T$ through (6),

$$f_p(z) = \left[ \sum_{k=1}^{n} \frac{\varphi_{k,p}(z)}{(z - s_{k,p})^{3/2}} \right]^2, \tag{8}$$

where $s_{k,p}$ are the singularities induced inside $D$ by the source $C_k$ and $\varphi_{k,p}$ are the smooth functions in $\overline{D}$.

The localization of $s_{k,p}$ then leads to that of $C_k$. Indeed, the complex argument of $s_{k,p}$ is independent of $p$ and equal to the argument of $z_k$, which allows us to determine the number $n$ of sources. Further, for fixed $k$, when $p$ varies, the quantity $r_p|s_{k,p}|$ attains its maximal value, equal to $|z_k|$, when $x_{3,k} = x_{3,p}$, in the slice $p$ corresponding to $C_k$.

Figure 5 shows the trajectories of the singularities $s_{k,p}$ in a two-source case.

[5] This is generically true with respect to plane $\Pi$. See however appendix B for the degenerated situation where $z_k = 0$.

### *3.3. Recovering 2D singularities*

This section deals with the computation of the singularities $s_{k,p}$ from the sliced boundary data $f_p$ on $T$, given by (7) at fixed $p$.

From formula (8), it can be seen that the function $f_p$ has the following properties.

- If there is a single source ($n = 1$), then $f_p$ is exactly a rational function with a single triple pole in $D$ at position $s_{1,p}$:

$$f_p(z) = \frac{\varphi_{1,p}^2(z)}{(z - s_{1,p})^3}. \tag{9}$$

- If there are multiple singularities ($n \geqslant 2$), $f_p$ is no longer a rational function (because of terms with power $3/2$ at the denominator of (8)). In this situation, the $s_{k,p}$ are both (triple) *poles* and *branchpoints* (of order $3/2$).[6] Yet, $f_p$ can be well approximated on the boundary $T$ by a rational function with poles in $D$; see appendix C and Baratchart *et al* (2006), and Baratchart and Yattselev (2009).

This gives rise to the following algorithm, which provides the estimates $\widehat{s_{k,p}}$ of $s_{k,p}$ from the sample values $\widehat{f_p}$ built from (7).

*Finding planar singularities* $\widehat{s_{k,p}} \simeq s_{k,p}$ *from cortical data* $\widehat{f_p}$

(i) Choose the number $n$ of sources.
(ii) Find initial values $s_{k,p}^*$ of $s_{k,p}$, to be the poles of a rational approximation $f_p^*$ of $f_p$ with appropriate degree (depending on $n$).
(iii) If $n = 1$ then $\widehat{s_{k,p}} = s_{k,p}^*$.
(iv) Otherwise, for $f_p$ linked to $s_{k,p}$ by (8) and starting with the initial values $s_{k,p}^*$, find $\widehat{s_{k,p}}$ by minimizing (gradient descent) the criterion:

$$\widehat{s_{k,p}} = \arg\min_{s_{k,p}} \left\| \widehat{f_p} - f_p \right\|.$$

**Remark 1.** Although it should become an output of the proposed method, the number $n$ is a necessary preliminary guess in the present algorithm.

In point (iv), $\| \ \|$ is the $l^2$ norm on $T$. The data $f_p$ are assumed to be given either by a number of its pointwise values on $T$, or by a number of its Fourier coefficients, using the spherical harmonics expansion of $u_a$ on $\mathbb{S}_0$ from section 3.1.2. From this Fourier expansion, we shall keep only the part with negative indices, for it is enough to account for the singularities of $f_p$ in $D$ (see appendix C.2.), which we still call $f_p$, for simplicity.

Strategies for achieving step (ii) of this algorithm are discussed in appendix C.

The present planar singularity detection step must be performed with several slicing directions $\Pi$, in order to get more accuracy on the localization process and to separate sources (see section 3.4 and Marmorat *et al* 2002, and Marmorat and Olivi 2004).

### *3.4. From estimated singularities to source positions and moments*

Given a slicing direction $\Pi$, the method described in section 3.3 provides estimates of the singularities $\widehat{s_{k,p}}$ of $f_p$ in each slice. But, we know from section 3.2 that the points $(r_p s_{k,p})_{k,p}$ are organized along as many lines $l_k$ as there are sources ($k = 1, \ldots, n$) (see the lines formed by the green (light grey) dots in figure 5).

[6] Recall that a pole (or polar singularity) is the zero of some polynomial at the denominator of the function, while a branchpoint is the singular point of some multivalued complex analytic function, as log or square root.

*3.4.1. Sources from a single slicing direction.* Each line $l_k$ is (generically, for most slicing directions) associated with one of the sources $C_k$ and has the following theoretical properties (from section 3.2).

(i) $l_k$ lies in a single half-plane $H_k$ defined by $C_k$ and by the direction of the slicing plane $\Pi$: $H_k$ contains $C_k$ and is orthogonal to $\Pi$.
(ii) $l_k$ goes through its associated source $C_k$. At this point, the radial distance of the line $l_k$ to the boundary of $H_k$ (the diameter of $\mathbb{S}_0$ orthogonal to $\Pi$) reaches its maximum.

The first property is used to group the points $r_p\widehat{s_{k,p}}$ into $n$ estimated lines $\widehat{l_k}$. To do so, these points are clustered in $n$ classes by applying Matlab's algorithm `clusterdata` to their polar angles. For each class, the best-fitting half-plane $\widehat{H_k}$ is then estimated using a least-squares algorithm and the points are reprojected on that plane, providing us with an estimation $\widehat{l_k}$ of the line $l_k$. The polar angle of $\widehat{H_k}$ is an approximation of the complex argument $\operatorname{Arg}\widehat{z_k}$ of $\operatorname{Arg} z_k$. We can now compute $|z_k|$ using the second above property as

$$\widehat{|z_k|} = \max_{p \in 1,\ldots,P} \{|r_p\widehat{s_{k,p}}| \text{ among } r_p\widehat{s_{k,p}} \in \widehat{l_k} \subset \widehat{H_k}\}.$$

We then obtain $\widehat{z_k}$ which, together with the argument $p$ of the above max, provides an estimate $\widehat{C_k}$ of the source positions, for direction $\Pi$.

*3.4.2. Combining information from multiple slicing directions.* The above procedure is repeated for a number $n_p$ of different slicing directions, which yields a family of $n_p \times n$ estimations of the $n$ source positions. Matlab's algorithm `clusterdata` is again used to build $n$ separate clusters from these $n_p \times n$ points. The final estimations $\widehat{C_k}$ of the sources are obtained as the barycenter of each cluster. As in the previous section, the distance between points is defined so as to ensure that each slicing direction contributes only once to each cluster.

Once the source positions are known, the measured potential is a linear function of the moments. These are thus estimated using a simple linear least-squares minimization procedure.

## 4. Numerical validation

We now present numerical results obtained with `FindSources3D`, a `Matlab` code that implements the above algorithm (Bassila *et al* 2008).

We simulated two datasets with `OpenMEEG`, which implements the symmetric boundary element method (Gramfort *et al* 2010, Kybic *et al* 2005). We considered data at the scalp level (potential measured by 128 electrodes), and also at the cortex level (potential and normal current on a 642-point mesh), in order to test the influence of the cortical mapping step on the quality of the source estimation. The spherical three-layer head model is the one described in section 2.1.

In the case of cortical data, that is, with potential and current at the cortex level as computed by `OpenMEEG`, figure 6 displays for 12 different slicing directions the top views of the planar detected singularities. Figure 7 shows the 3D superposition of all these estimated singularities for all axis directions and the estimated source positions for all the slicing directions.

Figure 8 displays true and estimated sources from the two datasets, while table 1 displays numerical values of the corresponding positions and moments.

We can see in figures 6–8 how the present numerical results illustrate theoretical properties established in section 3.3.

- For a given slicing direction $\Pi$, the singularities associated with a source $C_k$ lie in a plane $H_k$ containing the source itself and the slicing axis (figure 6).

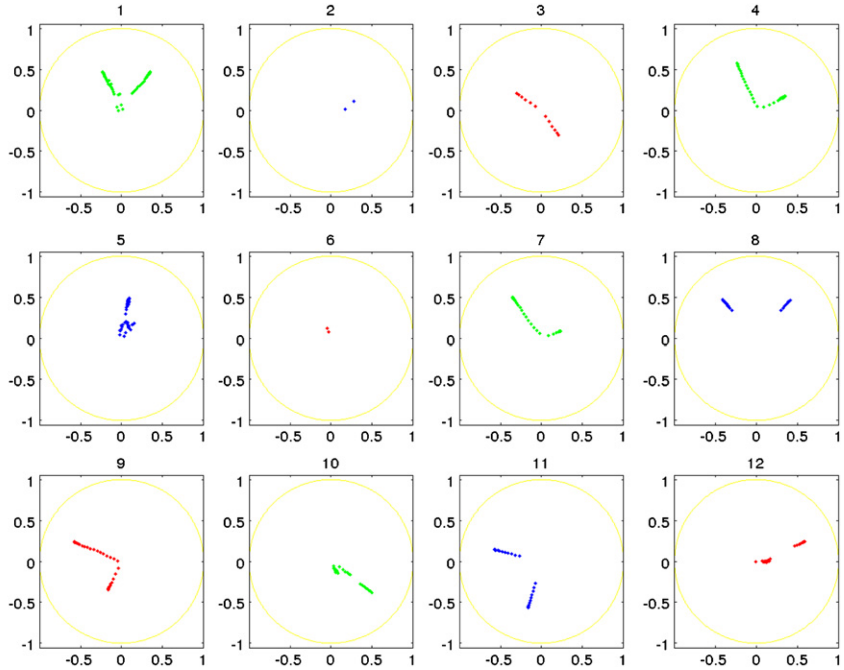

**Figure 6.** Top views of 2D planar singularities computed from the cortical dataset for 12 different slicing directions $\Pi$.

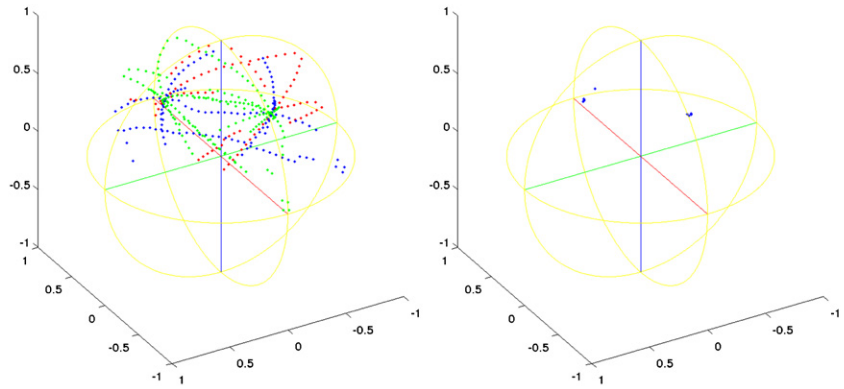

**Figure 7.** 3D superposition for different slicing directions: all singularities (left), estimated source positions $\widehat{C_k}$ for all slicing directions (right).

- As a consequence, singularity lines associated with various slicing directions $\Pi$ intersect at the sources, which allows us to estimate their positions (figure 7).
- Once these positions are estimated, the linear problem is easily solved to recover the source moments (figure 8).

As could be expected, estimation is better when data are directly taken at the cortical level on many points. The treatment of more realistic datasets (from scalp electrodes) needs an additional cortical mapping step and thus achieves a less precise estimation. However, the full

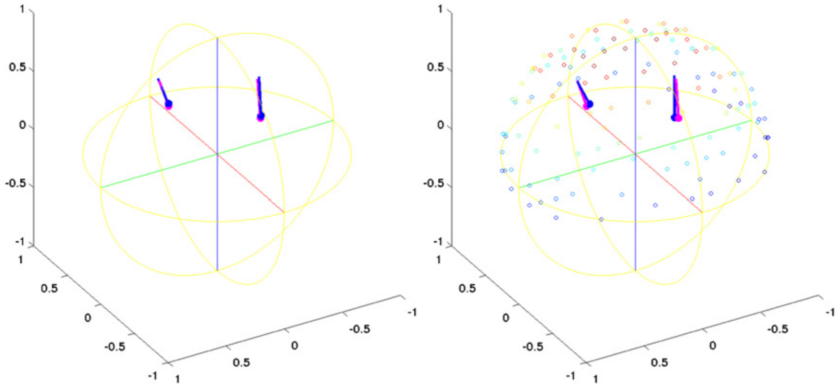

**Figure 8.** True versus estimated sources: cortical data (left), electrode data (right).

**Table 1.** True versus estimated sources from cortical and electrode datasets.

| | Positions | | | Moments | | |
|---|---|---|---|---|---|---|
| True sources | 0.2000 | 0.3000 | 0.4000 | 0.0000 | 0.2000 | 0.6000 |
| | −0.3000 | −0.2000 | 0.4000 | 0.1000 | 0.0000 | 0.8000 |
| Estimated sources | 0.1951 | 0.3056 | 0.4260 | 0.0194 | 0.2068 | 0.5874 |
| (cortical data) | −0.3006 | −0.2059 | 0.4208 | 0.0808 | −0.0052 | 0.7993 |
| Estimated sources | 0.1917 | 0.2797 | 0.4160 | 0.0112 | 0.2579 | 0.5563 |
| (electrode data) | −0.2798 | −0.1777 | 0.4015 | 0.0929 | −0.0486 | 0.8487 |
| Error | 0.0049 | −0.0056 | −0.0260 | −0.0194 | −0.0068 | 0.0126 |
| (cortical data) | 0.0006 | 0.0059 | −0.0208 | 0.0192 | 0.0052 | 0.0007 |
| Error | 0.0083 | 0.0203 | −0.0160 | −0.0112 | −0.0579 | 0.0437 |
| (electrode data) | −0.0202 | −0.0223 | −0.0015 | 0.0071 | 0.0486 | −0.0487 |

procedure proves to be efficient enough: when estimating sources from the electrode dataset, the global position error is less than 10% of the sphere radius (order of the cm).

## 5. Conclusion

We presented here some insights concerning the resolution of a source estimation problem. The techniques rely on constructive approximation; they are robust and efficient toward the EEG inverse source problem, as illustrated by preliminary numerics.

More accuracy on source localization may be achieved by extending the present method. A first possibility would be to take into account several time samples while constraining the source positions to be fixed. Also, the computation steps concerning the singular part of the cortical potential and its 3D to 2D transformation could be made more direct, in order to limit the numerical errors.

The number of unknown sources is not yet identified automatically. However, at many steps, information is available to build good estimates of this unknown number: singular values in the rational 2D approximation scheme, residual boundary approximation error, clustering procedure, etc. Work is in progress to make this number an output of the whole process, using techniques such as the Akaike information criterion to decide when increasing the number of sources is no longer significative with respect to the data.

Magnetic data from MEG (magnetoencephalography) will be incorporated as well, coupled to the available EEG, that may lead to additional precision in the source localization process.

Geometrically, the approach applies in principle to more general smooth 3D domains (Ebenfelt *et al* 2001), but we did not carry out such generalizations here and only considered spherical models. One may observe that whenever the complexity of the geometry increases, so does the quantity of planar singularities associated with a source. For an ellipsoidal domain, which has been theoretically studied in Leblond *et al* (2008), we already get two planar singularities for each source, in each ellipse.

**Acknowledgments**

The authors acknowledge partial support from the French National Research Agency, under the ANR grants AHPI, CoAdapt, ViMAGINE.

## Appendix A. Data transmission by cortical mapping

The cortical mapping method, originally presented in Clerc and Kybic (2007), proceeds as follows. With the rationale of the symmetric boundary element method (Kybic *et al* 2005), $u$ (resp. the normal current $\sigma\,\partial_\nu u$) is approximated with continuous, piecewise-linear elements (resp. discontinuous, piecewise-constant elements). The discretization of these two variables on each of the boundaries $\mathbb{S}_i$, $i = 0, 1, 2$, yields a set of values which are combined in a single-vector-valued variable $X$. The harmonic nature of $u$ in $\Omega_1 \cup \Omega_2$, along with the fact that $\partial_\nu u = 0$ on $\mathbb{S}_2$, and the transmission conditions (2) and (3) are all handled by saying that $X$ must belong to the kernel of a specific linear operator. This linear operator is represented by a dense matrix $H$, whose elements involve boundary integral operators. The knowledge of $u$ on $K$ is handled by a 'measurement operator' $M$, such that $MX$ represents $u_K$, i.e. the measurements on $K$. Ideally one would like to find $X$ such that $MX = u_K$ and $HX = 0$, but the ill-posedness of the Cauchy inverse problem makes it necessary to stabilize the system through a regularization. As a consequence, the method seeks $X$ belonging to the kernel of $H$ solving

$$\arg\min_{X\in\operatorname{Ker} H} \|MX - u_K\|^2 + \lambda\|RX\|^2.$$

The norms above are discrete $l^2$ norms, $\lambda$ is a real positive Lagrange parameter to be adjusted and $R$ is an appropriate regularization operator. Once the minimizer $X$ has been computed, it is immediate to extract from $X$ the desired transmitted data $u$ and $\sigma\,\partial_\nu u$ on $\mathbb{S}_0$. Results obtained by this method are illustrated in figure A1, where the two sources were taken as in section 3.1.2, and each sphere was meshed with 642 points. This figure shows the propagation of the potential measured on 128 electrodes onto the outer skull surface $\mathbb{S}_1$ and cortical surface $\mathbb{S}_0$.

Note that other transmission schemes can be obtained by best approximation with harmonic gradients, as in Atfeh *et al* (2010), and robust interpolation issues can be handled using spherical harmonics (Dautray and Lions 2000).

## Appendix B. Link between 3D sources and 2D singularities

Choose a fixed slicing direction $\Pi$, as in section 3.2. For $x \in T_p$ and $z \in T$ given by (6), let us establish equation (8) for $f_p$, which is equal to $u_a^2$ according to (7), where $u_a$ has been defined in (5). Indeed, with $h_{k,p} = x_{3,p} - x_{3,k}$,

$$|x - C_k|^2 = (x_1 - x_{1,k})^2 + (x_2 - x_{2,k})^2 + (x_{3,p} - x_{3,k})^2 = |r_p z - z_k|^2 + h_{k,p}^2;$$

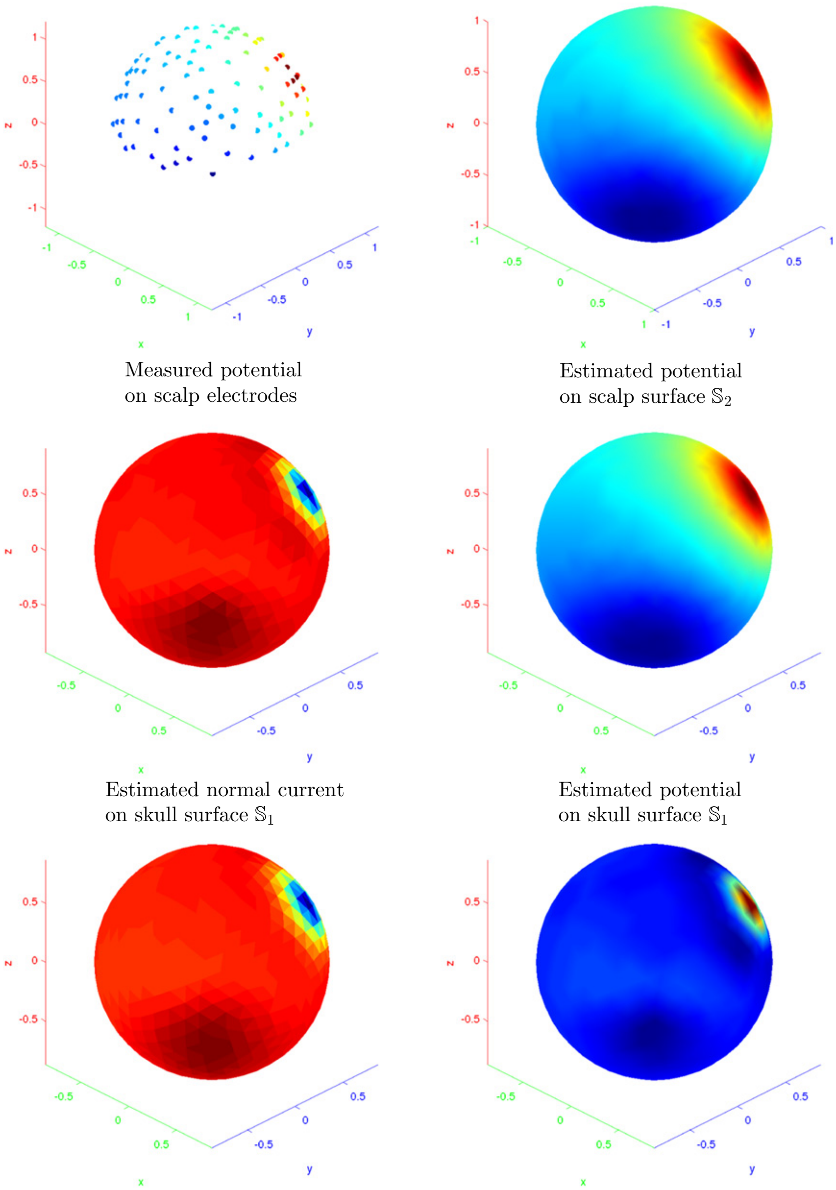


Measured potential on scalp electrodes

Estimated potential on scalp surface $\mathbb{S}_2$

Estimated normal current on skull surface $\mathbb{S}_1$

Estimated potential on skull surface $\mathbb{S}_1$

Estimated normal current on cortical surface $\mathbb{S}_0$

Estimated potential on cortical surface $\mathbb{S}_0$

**Figure A1.** Cortical mapping reconstruction. From the potential measured on 128 electrodes (top left), the cortical mapping method reconstructs the normal current and the potential on all surfaces of the model. The normal current is not represented on the scalp because it is simply equal to zero in our model. Note that the spatial distribution of the potential is less sharp on the scalp and skull surfaces (top right and middle right) than on the cortex, due to the high resistivity of the skull.

thus,

$$|x - C_k|^2 = (r_p z - z_k)(r_p \bar{z} - \bar{z}_k) + h_{k,p}^2 = (r_p z - z_k)\left(\frac{r_p}{z} - \bar{z}_k\right) + h_{k,p}^2$$

because $\bar{z} = 1/z$ for $z \in T$ (use that $|z|^2 = z\bar{z} = 1$). Assuming first that $z_k \neq 0$, we obtain

$$(r_p z - z_k)\left(\frac{r_p}{z} - \bar{z}_k\right) + h_{k,p}^2 = -\frac{r_p \bar{z}_k}{z}\left(z^2 - \frac{h_{k,p}^2 + |z_k|^2 + r_p^2}{r_p \bar{z}_k} z + \frac{z_k}{\bar{z}_k}\right).$$

Hence, for $x \in T_p$, $|x - C_k|^2$ coincides with the values on $T$ of the function defined in the whole of $\overline{D}$ by

$$-\frac{r_p \bar{z}_k}{z}(z - s_{k,p})(z - \sigma_{k,p}),$$

where the singularities $s_k = s_{k,p} \in D$ and $\sigma_k = \sigma_{k,p} \in \overline{D}$ are linked between each other and with the source parameters ($C_k$ being determined by the quantities $z_k$, $h_{k,p}$ and $r_p$) by the relations

$$\sigma_{k,p} = \frac{z_k}{\bar{z}_k s_{k,p}} \quad \text{and} \quad s_{k,p} = \frac{z_k}{2|z_k|^2 r_p}$$
$$\times \left(h_{k,p}^2 + r_p^2 + |z_k|^2 \sqrt{\left(h_{k,p}^2 + (r_p + |z_k|)^2\right)\left(h_{k,p}^2 + (r_p - |z_k|)^2\right)}\right).$$

Also, for each slice index $p = 1, \ldots, P$,

$$|s_{k,p}|\,|\sigma_{k,p}| = 1 \quad \text{and} \quad \arg s_{k,p} = \arg \sigma_{k,p} = \arg z_k. \tag{B.1}$$

With the standard convention that the square root is positive for positive arguments (which is used throughout the paper), $s_{k,p}$ is the root with the smallest modulus and (B.1) ensures that $s_{k,p} \in D$ while $\sigma_{k,p} \in \overline{D}$. Recalling (7) and (5), this leads to expression (8), or equivalently to

$$f_p(z) = \sum_{k=1}^{n} \frac{\varphi_{k,p}^2(z)}{(z - s_{k,p})^3} + 2 \sum_{\substack{k,j=1 \\ k \neq j}}^{n} \frac{\varphi_{k,p}(z)\varphi_{j,p}(z)}{(z - s_{k,p})^{3/2}(z - s_{j,p})^{3/2}}, \tag{B.2}$$

which shows that $f_p$ admits the singularities $s_{k,p}$ in $D$; see below for the functions $\varphi_{k,p}$ at the numerators. The above computation exposes two useful properties of $s_{k,p}$ which are used in section 3.4 toward the localization of $C_k$.

(i) The argument of the complex number $s_{k,p}$ is independent of $p$, and equal to the argument of $z_k$. In any slicing direction that separates the sources (that is if $z_k \neq z_j$ for $k \neq j$, which generically holds), this property allows us
- to determine the number of sources $n$, since the quantity of sources should be equal to the number of values taken by the complex argument of $s_{k,p}$, as $k$ and $p$ vary;
- for any fixed index $k_0$, to track $s_{k_0,p}$ among all the $s_{k,p}$ in any slice $p$ (the complex argument of $s_{k_0,p}$ does not depend on $p$);
- to determine the argument of $z_{k_0}$.

(ii) When $p$ varies (for $x_{3,p} \in (-1, 1)$), the modulus of $r_p\, s_{k,p}$ increases monotonically for $x_{3,p} < x_{3,k}$ (decreases monotonically for $x_{3,k} < x_{3,p}$) and attains a maximum when $x_{3,k} = x_{3,p}$ or $h_{k_0,p} = 0$, in which case one has $r_p\,|s_{k_0,p}| = |z_{k_0}|$. This second property allows us to determine $|z_{k_0}|$, whence finally $z_{k_0}$.

Also, if we put $p_k = (p_{1,k}, p_{2,k}, p_{3,k})$ for the moments and $\varrho_k = p_{1,k} + \mathrm{i}p_{2,k}$, we get from (5) that

$$\varphi_{k,p}(z) = \frac{1}{8\pi} \frac{\bar{\varrho}_k}{(r_p \bar{z}_k)^{3/2}} \frac{\sqrt{z}}{(\sigma_{k,p} - z)^{3/2}} \pi_{2,k,p}(z)$$

are uniformly bounded in $D$ and $\pi_{2,k,p}$ are polynomials of degree 2 (see also Baratchart *et al* (2006)):

$$\pi_{2,k,p}(z) = r_p z^2 + 2\frac{p_{3,k}h_{k,p} - \text{Re}\,(z_k\bar{\varrho}_k)}{\bar{\varrho}_k}z + \frac{\varrho_k}{\bar{\varrho}_k}r_p.$$

Finally, whenever $z_k = 0$ (that is, when the associated $C_k$ lies on the vertical axis), $|x - C_k|^2 = r_p^2 + h_{k,p}^2$ is a constant and the corresponding term of (8) becomes a rational function of $z$ which assumes the form $\pi_{2,k,p}(z)/z$ for the above-mentioned polynomials $\pi_{2,k,p}$. In this situation, the function $f_p$ to be approximated has a unique (double) pole in $D$ at 0, in every planar section $p$, which will be revealed by the rational approximation step. The sum of the roots of the polynomial $\pi_{2,k,p}$ is equal to $-\frac{2p_{3,k}}{\bar{\varrho}_k r_p}h_{k,p}$. If $p_{3,k} \neq 0$, the behavior of these roots still allows us to compute the index $p$ such that $h_{k,p} = 0$, and to finally locate the singularity $C_k$. The situation where $z_k = 0$ and $p_{3,k} = 0$ however is degenerated w.r.t. the present choice of $\Pi$, which is the reason why several slicing directions should be used.

## Appendix C. Best rational approximation schemes

### *C.1. Best rational approximation*

From the knowledge of $f_p$ on the surrounding circle $T$, the $s_{k,p}$ in $D$, $k = 1, \ldots, n$, are localized using rational approximation on $T$, with poles in $D$. Indeed, as we will see, the poles $s_{k,p}^*$ of such approximants accumulate to the singularities $s_{k,p}$ of the approximated function $f_p$.

Let us first briefly explain the best quadratic rational approximation techniques that are used.

As explained in section 3.3, the singularities $s_{k,p}$ can be described both as branchpoints and as triple poles of $f_p$. For a single source, we noted that $f_p$ is exactly a degree 3 rational function and the singularity $s_{k,p}$ is itself a triple pole. For multiple sources, the situation is not so simple, but the property that pole lines pass near the singularities still remains. This makes it interesting to consider two rational approximation schemes: one with simple poles and the other with triple poles.

We define $\mathcal{R}_m$ to be the set of rational functions $R_m$ with less than $m$ poles in $D$: $R_m = \frac{\pi_m}{q_m}$, where $\pi_m$ and $q_m$ are polynomials such that deg $\pi_m <$ deg $q_m \leqslant m$, and where the zeroes of $q_m$ belong to $D$.

A best quadratic rational approximant to $f_p$ in $\mathcal{R}_m$ is a function $R_m^* \in \mathcal{R}_m$, verifying

$$\left\| f_p - R_m^* \right\| = \min_{R_m \in \mathcal{R}_m} \| f_p - R_m \|, \tag{C.1}$$

for the $L^2(T)$ norm, see Baratchart *et al* (1992). Existence and non-uniqueness of $R_m^*$ are discussed in Baratchart *et al* (1992). Concerning constructive aspects, efficient algorithms to generate local minima are obtained using Schur parametrization (Marmorat *et al* 2002). Computation of $R_m^*$ is made effective through suitable parametrization of rational functions, using gradient algorithms (Marmorat *et al* 2002).

Generally and properly speaking, for functions $f_p \in L^2(T)$, the approximation class $\mathcal{R}_m$ should be the set of 'meromorphic' functions with less than $m$ poles in $D$. Such a meromorphic function is the sum of a rational function $\frac{\pi_m}{q_m}$ and of a function $h$ 'holomorphic' (or equivalently 'analytic') in $D$ (which has no singularities in $D$ but may have poles outside $D$). Because

$$\frac{\pi_m}{q_m} + h = \frac{\pi_m + hq_m}{q_m},$$

we see that a meromorphic function coincides with the quotient of a holomorphic function by a polynomial.

Further, whenever $f_p$ has singularities only in $D$ and is analytic in $\mathbb{C} \setminus \overline{D}$ (and vanishes at $\infty$), its best meromorphic approximant coincides with its best rational approximant with poles in $D$. This is the reason why we explain in appendix C.2. how to get, in general, this part of $f_p$, analytic in $\mathbb{C} \setminus \overline{D}$, which shares the singularities of $f_p$ in $D$ but as no singularity outside $D$.

### *C.2. 2D analytic projection*

Observe from appendix B that $f_p$ possesses singularities both inside and outside the unit disk, which are linked to each other and to the sources $C_k$, see e.g. (B.1).

Indeed, representation (8) involves the singularities $s_{k,p}$ of $f_p$ in $D$ but also the additional reflected ones $\sigma_{k,p}$ (hidden in $\varphi_{k,p}$) outside $D$. First, these are linked with each other by (B.1). Next, the rational approximation algorithms available for data on $T$ require the singularities of the approximated functions to belong to a region of the plane limited by $T$ (see section 3.3; in particular, this leads to a lower degree of the approximants, which also possess strong robustness properties). We thus choose to keep only those of the singularities $s_{k,p}$ of $f_p$ that belong to the disk $D$, and we need to filter the $\sigma_{k,p}$ out.

It is easily seen from (8) that the function $f_p$ is continuous on $T$, because none of its singularities belong to $T$. Thus, it belongs to the Lebesgue space $L^2(T)$ of functions with square summable modulus on $T$. Consequently, it can be uniquely written on $T$ as the sum $f_p = F + F_o$, where $F$ is the holomorphic projection of $f_p$ in $\mathbb{C} \setminus \overline{D}$ and vanishes at $\infty$, while $F_o$ is holomorphic in $D$. Actually, $F$ and $F_o$ respectively belong to the Hardy classes of $\mathbb{C} \setminus \overline{D}$ and of $D$, their traces on $T$ belonging to $L^2(T)$ (Rudin 1987). The Hardy–Hilbert spaces $H^2_-$, resp. $H^2_+$, are the sets of functions analytic in $\mathbb{C} \setminus \overline{D}$ (vanishing at $\infty$), resp. analytic in $D$, and bounded in $L^2(T)$ norm (i.e. the space of $L^2(T)$ functions with vanishing Fourier coefficients of positive indices, resp. of strictly negative indices). We can directly compute $F$ from the Fourier series expansion of $f_p$ on $T$:

$$f_p(\mathrm{e}^{\mathrm{i}\theta}) = \sum_{l\in\mathbb{Z}} F_l \mathrm{e}^{\mathrm{i}l\theta}, \quad \sum_{l\in\mathbb{Z}} |F_l|^2 < \infty \Rightarrow F(z) = (P_- f_p)(z) = \sum_{l<0} F_l z^l, \quad |z| \geqslant 1, \qquad \text{(C.2)}$$

if $P_-$ denotes the orthogonal 'anti-analytic' projection from $L^2(T)$ onto $H^2_-$. The important point here is that $f_p$ and $F$ share the same singularities inside $D$, while $F$ has no singularities outside $D$, since $F$ possesses an expression analogous to (8), with identical denominators, but numerators given by smooth functions. This is necessary for the best rational approximation problem to be solved among rational (no longer meromorphic) functions with poles in $D$.

We shall then assume from now on, and already for the computations of section 3.3, that $f_p$ is analytic in $\mathbb{C} \setminus \overline{D}$, and vanishes at $\infty$, without loss of generality.

### *C.3. Behavior of simple poles with respect to singularities and sources*

If the degree $m$ is not preliminarily given, observe that its estimation can be obtained by computing the boundary error on $T$ (the value of the criterion in (C.1)) for increasing values of $m$, until it is small enough, see remark 1. This will happen in principle for $m \simeq 3\,n$, the number of singularities of $f_p$ in $D$ according to their multiplicity.

For such a value of $m$, compute the best approximant $R^*_m$ itself (that the approximant should be computed only once, for $m$ large enough for the error to be sufficiently small, is one of the features that make this scheme efficient).

In sections $p$ close to $C_k$, $f_p$ is (numerically) close to a rational function with poles at $(s_{k,p})$. Thus, for $m$ large enough, typically $m \geqslant 3n$, the $m$ poles of $R^*_m$ must then be located near the $(s_{k,p})$ (see property (P), appendix C.5.), and they should be packed in a number of clusters coinciding with the number $n$ of sources.

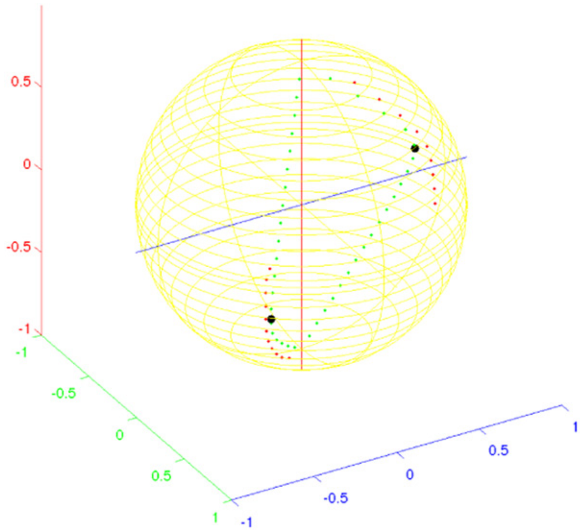


**Figure C1.** One simple pole.

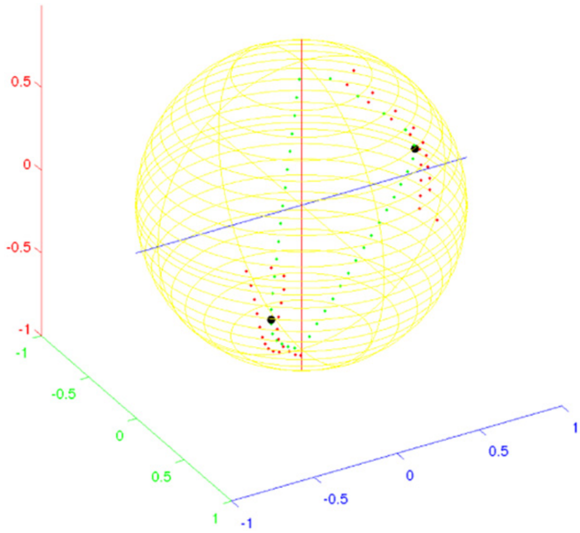


**Figure C2.** Two simple poles.

This is illustrated in figures C1–C3 where $m = 1, 2$ and 3 simple poles cases are respectively shown for the same situation with $n = 2$ sources as in section 3.1.2. For $k = 1, 2$ and varying $p$, theoretically known singularities $(r_p s_{k,p})$ are shown in disks $D_p$ as green (light grey) dots, whereas estimated poles are shown with red (dark grey) dots. The large black dots represent the sources $C_1, C_2$.

### *C.4. Behavior of triple poles with respect to singularities and sources*

Recall that the singularities $s_{k,p}$ that we aim to recover appear at *triple* poles of $f_p$, from (8), which motivates the computation of the best rational approximants with *triple* poles.

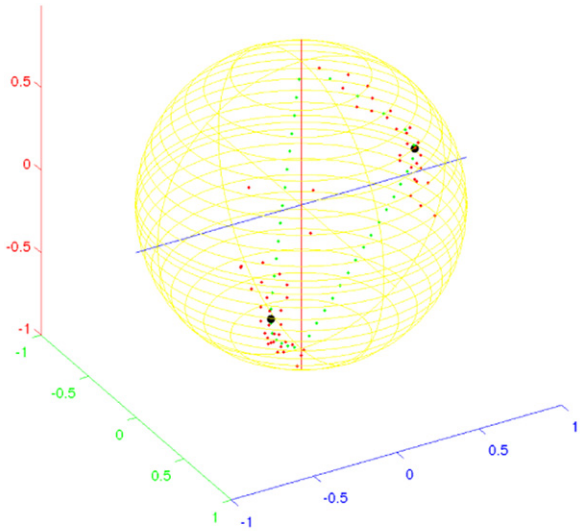


**Figure C3.** Three simple poles.

Recall that for a single source ($n = 1$), (8) is to the effect that $f_p$ is a rational function with a triple pole in $D$, see (9). Hence, its best rational approximant with a single triple pole in $D$ should coincide with $f_p$ itself. Whenever $n > 1$, the situation is of course more complicated since $f_p$ admits the $s_{k,p}$ both as triple poles and branchpoints. However, as we shall see, the behavior of poles dominates whence its best rational approximant with triple poles still allows us to recover the $s_{k,p}$.

These best rational approximants with triple poles in $D$ are functions $R^*_{3m} = \pi_{3m}/q^3_m \in \mathcal{R}_{3m}$ that satisfy (C.1), where $\pi$ and $q$ are polynomials such that deg $q_m \leqslant m$, deg $\pi_{3m} < 3m$. An advantage is that the computations can then be performed with a lower degree than in the simple poles case, since $m = n$ is enough.

Again, even though $f_p$ is not a rational function (it admits poles *and branchpoints located at the same place*), it is (numerically) close to rationals of $\mathcal{R}_3$ with *a single triple pole* ($m = 1$), in plane sections $p$ close to the one containing $(C_k)$, even for several sources, when $n > 1$.

For such data $f_p$, close to a rational function of $\mathcal{R}_3$ with a single triple pole, say $t$, in $D$, the single triple pole of the best rational approximant is close to $t$, see the robustness property (P′), appendix C.6.

Hence, the above best approximants $R^*_{3m}$ possess an even stronger property: in general a single ($m = 1$) triple pole is enough in order to localize several singularities $s_{k,p}$ in $D$, hence several sources $(C_k)$ ($n \geqslant 1$), by varying $p$. Indeed, in the slice $p$ containing a source $C_k$, the single triple pole $s^*_p$ of $R^*_3$ is close to the associated singularity $s_{k,p}$.

This situation is illustrated in figure C4 for the same source configuration as the one used for figures C1–C3. As previously, sources are indicated with large black dots, the green (light grey) dots show the known theoretical positions of singularities, while the red (dark grey) dots show the triple poles. One can note that there is only one pole trajectory for both singularity lines. Thus, the triple pole line does not follow the singularity lines as in the single-pole case. However, close to sources, the triple poles approximate the singularity lines quite well.

### *C.5. Behavior of simple poles of rational approximants*

We give a few additional considerations concerning the asymptotic behavior of the poles.

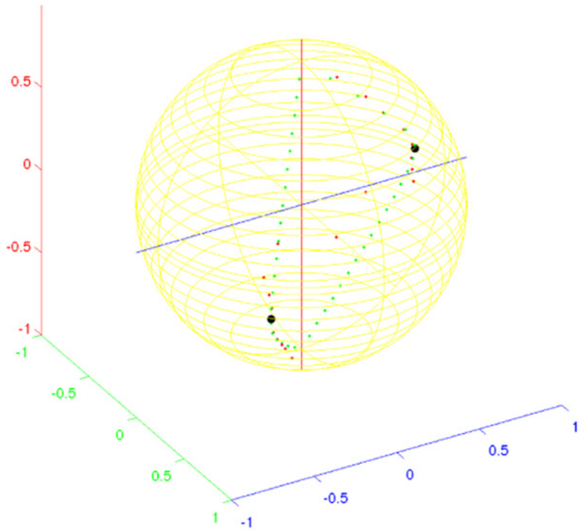


**Figure C4.** One triple pole.

In situations where $f_p$ is already a rational function $R_N$ of $\mathcal{R}_N$, its best rational approximant $R_m^*$ coincides with $f_p$ for $m \geqslant N$. This result is robust in the sense of property (P) below. Observe that whenever $n \geqslant 2$, the function $f_p$ has poles *and* branchpoints in $D$, and it can be shown that the degree of the denominator $q_m$ of $R_m^*$ is in fact equal to $m$, for each integer $m$. Property (P) can be deduced from Baratchart (1986) (property 5).

(P) *Whenever $f_p$ is close (in $L^2(T)$) to a rational function $R_N$, the poles of $R_m^*$ accumulate to those of $R_N$, as m increases.*

Further, deep convergence results from potential theory (Baratchart and Yattselev 2009) assert that, for a function $f_p$ as in the present situation (which admits finitely many poles and branchpoints in $D$ and has a smooth behavior near $T$), the $m$ poles of $R_m^*$ converge (in some weak sense) to the singularities $(s_k) = (s_{k,p})$ of $f_p$ as $m$ increases (where, for notational simplicity, the index $p$ is fixed and has been omitted).

For $n = 2$, the sequence of counting probability measures of the poles of $R_m^*$ will asymptotically charge $s_1$ and $s_2$ (the poles will accumulate 'near' $s_1$ and $s_2$), while only finitely many poles stay away from $s_1$, $s_2$ and from the arc of circle orthogonal to $T$ joining them (Baratchart *et al* 2001).

These results are related to the fact that, for $n = 2$, $f_p$ can be represented as

$$f_p(z) = R_6(z) + R_2(z) \int_{s_1}^{s_2} \frac{\mathrm{d}t}{(z-t)\sqrt{(t-s_1)(s_2-t)}},$$

for rationals $R_2 \in \mathcal{R}_2$ and $R_6 \in \mathcal{R}_6$ with, respectively, two simple poles for $R_2$ and two triple poles for $R_6$, at $s_1$ and $s_2$. This result is used in Baratchart and Yattselev (2009) to study the behavior of the poles of best rational approximants.

## *C.6. Behavior of triple poles of rational approximants*

We have the following robustness property.

(P′) *For a function $f_p$, close to a rational of $\mathcal{R}_3$ with a single triple pole $t \in D$, the triple pole $t^*$ of its best rational approximant $R_3^*$ (with a single triple pole in D) and t are close to each other.*

Property (P′) is a restatement of the following.

**Proposition 1.** *Let $R_3(z) = \pi(z)/(z-t)^3$ be a rational function of $\mathcal{R}_3$ with a triple pole $t \in D$, strictly proper ($\deg\pi < 3$), and irreducible ($\pi(s) \neq 0$). Then, there exists $K > 0$ such that for all rational function $\tilde{R}_3(z) = \tilde{\pi}(z)/(z-b)^3$ with a triple pole $b \in D$, the following inequality holds: $|t-b| \leqslant K\|R_3 - \tilde{R}_3\|$, for the $L^2(T)$ norm.*

Indeed, as a corollary, if $\|f_p - R_3\| \leqslant \epsilon$ (in $L^2(T)$ norm), for some $\epsilon > 0$ and $R_3 \in \mathcal{R}_3$ with a single triple pole $t$ in $D$, then we have the inequality $|t - t^*| < K\epsilon$.

**Proof of proposition 1.** Let $R = \pi/q$ and $\tilde{R} = \tilde{\pi}/\tilde{q}$ be two proper rational (irreducible) functions in $L^2(T)$: in particular, $\pi, q, \tilde{\pi}, \tilde{q}$ are polynomials, and the roots of $q$ and $\tilde{q}$ lie inside the open unit disk $D$ ($q$ and $\tilde{q}$ are called 'stable' polynomials). □

**Step 1.** We look for a lower bound to

$$\mathrm{d}(R, \tilde{R}) = \left\| \frac{\pi}{q} - \frac{\tilde{\pi}}{\tilde{q}} \right\|$$

($L^2(T)$ norm). If $n$ is the degree of $\tilde{q}$, put $\check{\tilde{q}}(z) = z^n\overline{\tilde{q}(1/\bar{z})}$ for its reciprocal polynomial. Then $\tilde{q}/\check{\tilde{q}}$ has modulus 1 on the unit circle, and we also have

$$\mathrm{d}(R, \tilde{R}) = \left\| \frac{\pi}{q}\frac{\tilde{q}}{\check{\tilde{q}}} - \frac{\tilde{\pi}}{\check{\tilde{q}}} \right\|.$$

From the orthogonal decomposition of $L^2(T)$ into Hardy spaces of analytic functions (Rudin 1987), and because $P_-(\tilde{\pi}/\check{\tilde{q}}) = 0$, since the poles of $\tilde{\pi}/\check{\tilde{q}}$ belong to $\mathbb{C} \setminus \overline{D}$, we get that

$$\mathrm{d}(R, \tilde{R}) \geqslant \left\| P_-\left(\frac{\pi}{q}\frac{\tilde{q}}{\check{\tilde{q}}}\right) \right\|. \tag{C.3}$$

**Remark 2.** The right-hand side of (C.3) vanishes if and only if $q$ is a divisor of $\tilde{q}$.

**Step 2.** In the particular case where $R \in \mathcal{R}_3$ and $\tilde{R}$ have a single triple pole respectively at $t \in D$, and at $b \in D$, then $q(z) = (z-t)^3$, $\tilde{q}(z) = (z-b)^3$, $\check{\tilde{q}}(z) = (1-\bar{b}z)^3$, and we can evaluate this right-hand side by a fractional decomposition. Indeed, expand $\pi(z)\tilde{q}(z)$ in powers of $(z-t)$ in order to obtain

$$P_-\left(\frac{\pi}{q}\frac{\tilde{q}}{\check{\tilde{q}}}\right) = P_-\left(\frac{1}{(1-\bar{b}z)^3}\left(\frac{A_1}{z-t} + \frac{A_2}{(z-t)^2} + \frac{A_3}{(z-t)^3}\right)\right) \tag{C.4}$$

with

$$A_1 = 3\pi(s)(t-b) + 3\pi'(t)(t-b)^2 + \pi''(t)(t-b)^3/2,$$
$$A_2 = 3\pi(s)(t-b)^2 + \pi'(t)(t-b)^3, \qquad A_3 = \pi(t)(t-b)^3.$$

Expanding now $1/\check{\tilde{q}}$ in a neighborhood of $z = t$ in $D$, we obtain

$$\frac{1}{\check{\tilde{q}}(z)} = \frac{1}{(1-\bar{b}z)^3} = \frac{1}{(1-\bar{b}s)^3}\left(1 + \frac{3\bar{b}(z-t)}{1-\bar{b}t} + \frac{6\bar{b}^2(z-t)^2}{(1-\bar{b}t)^2}\right) + O((z-t)^3).$$

The $P_-$ projections in (C.4) can then be expressed as

$$P_-\left(\frac{1}{(1-\bar{b}z)^3}\frac{1}{z-t}\right)=\frac{\alpha}{z-s},$$
$$P_-\left(\frac{1}{(1-\bar{b}z)^3}\frac{1}{(z-t)^2}\right)=\frac{\alpha}{(z-t)^2}+\frac{\beta}{z-t},$$
$$P_-\left(\frac{1}{(1-\bar{b}z)^3}\frac{1}{(z-t)^3}\right)=\frac{\alpha}{(z-t)^3}+\frac{\beta}{(z-t)^2}+\frac{\gamma}{z-t},$$

where

$$\alpha=\frac{1}{(1-\bar{b}t)^3},\qquad \beta=\frac{3\bar{b}}{(1-\bar{b}t)^4},\qquad \gamma=\frac{6\bar{b}^2}{(1-\bar{b}t)^5}.$$

Thus,

$$P_-\left(\frac{\pi}{q}\frac{\tilde{q}}{\check{\tilde{q}}}\right)=\Phi_{t,b}(z)=(t-b)\frac{N_{t,b}(z)}{(z-t)^3}=(t-b)\Psi_{t,b}(z),$$

where $\Phi_{t,b}$, $\Psi_{t,b}$ are rational functions, and $N_{t,b}$ is a polynomial of degree 2, as follows from

$$\Phi_{t,b}(z)=\frac{\alpha A_3}{(z-t)^3}+\frac{\alpha A_2+\beta A_3}{(z-t)^2}+\frac{\alpha A_1+\beta A_2+\gamma A_3}{z-t}.$$

Using (C.3), we thus obtain

$$\mathrm{d}(R,\tilde{R})\geqslant\|\Phi_{t,b}\|.$$

Note that $\Phi_{t,b}$, $\Psi_{t,b}$ and $N_{t,b}$ have continuous coefficients in the variable $b\in D$. In particular, for $b=t\in D$,

$$\Phi_{t,t}(z)=0,\qquad \Psi_{t,t}(z)=\frac{3\tilde{\pi}(t)}{(1-|t|^2)^3}\frac{1}{z-t}.$$

**Step 3.** Consider the $L^2(T)$ norms of $\Phi_{t,b}$ and $\Psi_{t,b}$ as functions of $b$, and put

$$\phi(b)=\|\Phi_{t,b}\|,\quad \psi(b)=\|\Psi_{t,b}\|,\quad \text{whence } \phi(b)=|t-b|\psi(b).$$

From (C.3), we now have that

$$\mathrm{d}(R,\tilde{R})\geqslant\phi(b).$$

The above expressions are then to the effect that $\phi$ and $\psi$ are continuous functions of $b\in D$. Further, $\phi$ and $\psi$ admit continuous extensions up to the closed disk $\overline{D}$, and $\psi$ does not vanish on $\overline{D}$. Indeed, let $|b|=1$ and $b_n\in D$, $b_n\to b$. Then, $\forall z\in D$, $\tilde{q}_n(z)/\check{\tilde{q}}_n(z)=(z-b_n)^3/(1-\bar{b}_nz)^3$ converges to the constant $-b^3$, whence $(\pi\tilde{q}_n)/(q\check{\tilde{q}}_n)\to -b^3\tilde{\pi}/\tilde{q}$ in $L^2(T)$. Since $P_-(\pi/q)=\pi/q=R$ (because $\mathcal{R}_m$ is contained in the above-mentioned Hardy class of functions analytic in $\mathbb{C}\setminus\overline{D}$ and by definition), we deduce that $\phi$ continuously extends to $T$ and that $\phi(b)=\|R\|$, $\forall b\in T$. Hence, $\psi$ also admits a continuous extension on $T$ and $\psi(b)=\|R\|/|t-b|$, $\forall b\in T$.

**Step 4.** Finally, the continuous positive function $\psi$ attains its minimal value $K'\geqslant 0$ in $\overline{D}$ at some point $b_0\in\overline{D}$. In order to establish by contradiction that $K'>0$, assume that $K'=0$; then $\psi(b_0)=0$ which implies $\phi(b_0)=0$. Then $b_0\notin T$, since $\phi_{|_T}=\|R\|$. But if $b_0\in D$, then necessarily $b_0=t$, the unique point in $D$ where $\phi$ vanishes, from remark 2. However, because $\left\|\frac{1}{z-t}\right\|=(1-|t|^2)^{-\frac{1}{2}}$, we have $\psi(t)=3|\tilde{\pi}(t)|(1-|t|^2)^{-\frac{7}{2}}$. Because $R=\pi/q$ is irreducible, then $\pi(t)\neq 0$, so $\psi(t)\neq 0$, and this is a contradiction. Hence, $K'>0$.

**Step 5.** Thus, $\psi(b)\geqslant K'>0$ whence, with $K=1/K'$, $\phi(b)\geqslant|t-b|$ and

$$|t-b|\leqslant K\phi(b)\leqslant K\,\mathrm{d}(R,\tilde{R}),$$

which achieves the proof of proposition 1, with $R_3=R$.

**Remark 3.** The expressions of $\alpha, \beta, \gamma$ lead to a similar result for the hyperbolic distance:

$$\exists K_0 > 0, \qquad \left|\frac{t-b}{1-\bar{b}t}\right| \leqslant K_0\phi(b) \leqslant K_0\,\mathrm{d}(R,\tilde{R}).$$

## References


Alessandrini G, Rondi L, Rosset E and Vessella S 2009 The stability for the Cauchy problem for elliptic equations *Inverse Problems* **25** 123004

Atfeh B, Baratchart L, Leblond J and Partington J R 2010 Bounded extremal and Cauchy–Laplace problems on the sphere and shell *J. Fourier Anal. Appl.* **16** 177–203

Baratchart L 1986 Existence and generic properties for $L^2$ approximants of linear systems *IMA J. Math. Control Identification* **3** 89–101

Baratchart L, Ben Abda A, Ben Hassen F and Leblond J 2005 Recovery of pointwise sources or small inclusions in 2D domains and rational approximation *Inverse Problems* **21** 51–74

Baratchart L, Leblond J and Marmorat J-P 2006 Inverse source problem in a 3D ball from best meromorphic approximation on 2D slices *Electron. Trans. Numer. Anal.* **25** 41–53

Baratchart L, Olivi M and Wielonsky F 1992 On a rational approximation problem in the real Hardy space $H_2$ *Theor. Comput. Sci.* **94** 175–97

Baratchart L, Stahl H and Wielonsky F 2001 Asymptotic uniqueness of best rational approximants of given degree to Markov functions in $L^2$ of the circle *Constructive Approx.* **17** 103–38

Baratchart L and Yattselev M 2009 Meromorphic approximants to complex Cauchy transforms with polar singularities *Mat. Sb.* **200** 3–40

Bassila R, Clerc M, Leblond J, Marmorat J-P and Papadopoulo T 2008 FindSources3D, http://www-sop.inria.fr/apics/FindSources3D/

Ben Abda A, Ben Hassen F, Leblond J and Mahjoub M 2009 Sources recovery from boundary data: a model related to electroencephalography *Math. Comput. Modelling* **49** 2213–23

Bénar C-G, Gunn R N, Grova C, Champagne B and Gotman J 2005 Statistical maps for EEG dipolar source localization *IEEE Trans. Biomed. Eng.* **52** 401–13

Clerc M and Kybic J 2007 Cortical mapping by Laplace–Cauchy transmission using a boundary element method *Inverse Problems* **23** 2589–601

Cuffin B 1995 A method for localizing EEG sources in realistic head models *IEEE Trans. Biomed. Eng.* **42** 68–71

Dautray R and Lions J-L 2000 *Mathematical Analysis and Numerical Methods for Science and Technology* vol 2 (Berlin: Springer)

Ebenfelt P, Khavinson D and Shapiro H S 2001 An inverse problem for the double layer potential *Comput. Methods Funct. Theory* **1** 387–402

El Badia A 2005 Inverse source problem in an anisotropic medium by boundary measurements *Inverse Problems* **21** 1487–506

El Badia A and Ha-Duong T 2000 An inverse source problem in potential analysis *Inverse Problems* **16** 651–63

Gramfort A, Papadopoulo T, Olivi E and Clerc M 2010 OpenMEEG: opensource software for quasistatic bioelectromagnetics *Biomed. Eng. OnLine* **9** 45

Isakov V 1998 *Inverse Problems for Partial Differential Equations* (*Applied Mathematical Sciences* vol 127) (Berlin: Springer)

Kandaswamy D, Blu T and Van De Ville D 2009 Analytic sensing: noniterative retrieval of point sources from boundary measurements *SIAM J. Sci. Comput.* **31** 3179–319

Kozlov V A, Mazya V G and Fomin A V 1992 An iterative method for solving the Cauchy problem for elliptic equations *Comput. Math. Math. Phys.* **31** 45–52

Kybic J, Clerc M, Abboud T, Faugeras O, Keriven R and Papadopoulo T 2005 A common formalism for the integral formulations of the forward EEG problem *IEEE Trans. Med. Imaging* **24** 12–28

Leblond J, Paduret C, Rigat S and Zghal M 2008 Source localisation in ellipsoids by best meromorphic approximation in planar sections *Inverse Problems* **24** 035017

Marmorat J-P and Olivi M 2004 Rational approximation: RARL2 (http://www-sop.inria.fr/apics/RARL2/rarl2-eng.html)

Marmorat J-P, Olivi M, Hanzon B and Peeters R L M 2002 Matrix rational $H^2$ approximation: a state-space approach using Schur parameters *Proc. CDC'02 (Las Vegas, NV)* pp 4244–9

Mosher J C, Lewis P S and Leahy R M 1992 Multiple dipole modeling and localization from spatio-temporal MEG data *IEEE Trans. Biomed. Eng.* **39** 541–53

Phung K D 2003 Remarques sur l'observabilité pour l'équation de laplace *ESAIM: COCV* **9** 621–35

Rudin W 1987 *Real and Complex Analysis* (New York: McGraw-Hill)

Scherg M, Bast T and Berg P 1999 Multiple source analysis of interictal spikes: goals, requirements, clinical value *J. Clin. Neurophysiol.* **16** 214–38

Van Veen B D and Buckley K M 1988 Beamforming: a versatile approach to spatial filtering *IEEE Acoust. Speech Signal Process Mag.* **5** 4–24

Vessella S 1992 Locations and strengths of point sources: stability estimates *Inverse Problems* **8** 911–7

Zghal M 2010 Problèmes inverses pour l'équation de Laplace en dimension 3, application à l'éléctroencéphalographie *PhD Thesis* ENIT, University Tunis El Manar